TECHNICAL REPORT BRL-TR-3172

BRL

COMPUTATION OF THE ROLL CHARACTERISTICS OF THE M829 KINETIC ENERGY PROJECTILE AND COMPARISON WITH RANGE DATA

PAUL WEINACHT
WALTER B. STUREK

NOVEMBER 1990

U.S. ARMY LABORATORY COMMAND

BALLISTIC RESEARCH LABORATORY
ABERDEEN PROVING GROUND, MARYLAND

DISCLAIMER NOTICE

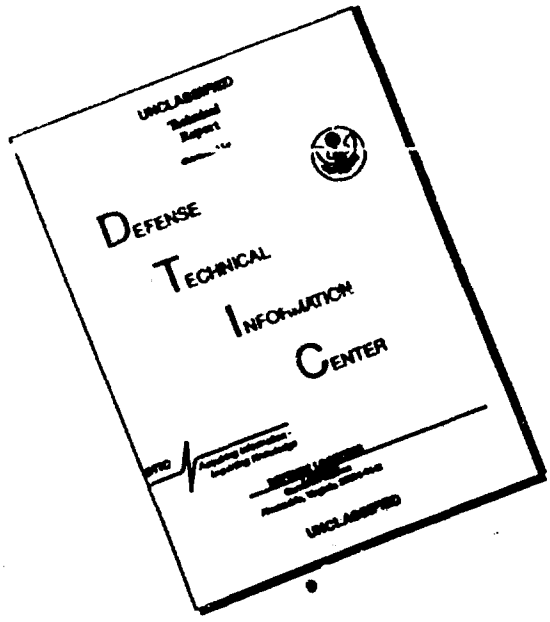

THIS DOCUMENT IS BEST QUALITY AVAILABLE. THE COPY FURNISHED TO DTIC CONTAINED A SIGNIFICANT NUMBER OF PAGES WHICH DO NOT REPRODUCE LEGIBLY.

NOTICES

Destroy this report when it is no longer needed. DO NOT return it to the originator.

Additional copies of this report may be obtained from the National Technical Information Service, U.S. Department of Commerce, 5285 Port Royal Road, Springfield, VA 22161.

The findings of this report are not to be construed as an official Department of the Army position, unless so designated by other authorized documents.

The use of trade names or manufacturers' names in this report does not constitute indorsement of any commercial product.

DEPARTMENT OF THE ARMY
UNITED STATES ARMY LABORATORY COMMAND
BALLISTIC RESEARCH LABORATORY
ABERDEEN PROVING GROUND, MARYLAND 21005-5066

REPLY TO
ATTENTION OF

SLCBR-DD-S

6 March 1991

MEMORANDUM FOR Defense Technical Information Center, ATTN: DTIC-HAS (Mr. Victor Furtado), Cameron Station, Alexandria, VA 22304-6145

SUBJECT: Technology Screening of Unclassified/Unlimited Reports

1. References:

a. Letter, DTIC-HAS, 22 February 1991, subject as above.

b. BRL Technical Report No. 3172, "Computation of the Roll Characteristics of the M829 Kinetic Energy Projectile and Comparison with Range Data."

2. Security, foreign intelligence and subject area experts reviewed reference 1b prior to publication and determined that it meets the criteria for public relase.

3. Point of contact is Mr. Douglas J. Kingsley, telephone 301-278-6960.

FOR THE DIRECTOR:

P. Ann Brown

P. ANN BROWN
Chief, Security Office

re-input

A227450

DEFENSE LOGISTICS AGENCY
DEFENSE TECHNICAL INFORMATION CENTER
CAMERON STATION
ALEXANDRIA, VIRGINIA 22304-6145

REPLY
REFER TO

DTIC-HAS

22 FEB 1991

SUBJECT: Technology Screening of Unclassified/Unlimited Reports

TO: Commander
U.S. Laboratory Command
Ballistic Research Laboratory
ATTN: SLCBR-DD-T
Aberdeen Proving Ground, MD 21005-5066

1. DTIC has been authorized by DoD to screen and challenge Distribution Statement "A" reports for security and critical technology that should be withheld from public sale through NTIS. Such reports will be available from DTIC only to its registered users.

2. The report referenced below has been received at DTIC and has been screened for security and technology control. The report is believed to contain technical data that should be denied public disclosure according to DoD Directive 5230.25, Withholding of Unclassified Technical Data from Public Disclosure.

Source: Ballistic Research Laboratory
Title: Computation of the Roll Characteristics of the M829 Kinetic Energy Projectile and Comparison with Range Data
Report No. BRL-TR-3172
Date of Report: November 1990

Applicable MCTL Ref.: Page 6-15, Paragraphs 6.4.2.A.1.a. and b.

3. The report will not be released to NTIS or DTIC users until the situation is resolved. Please review the report in accordance with the MCTL reference (cited above). Notify DTIC within 30 days whether the report meets the criteria for public release. If the report has already been exported (released to a foreign national or country), or if there is no response, DTIC will process the report by assigning the Distribution Statement "C": "Distribution limited to U.S. Government Agencies and their Contractors because of Critical Technology (DoD Directive 5230.24)." If the report has not been exported, DTIC will mark the report Statement "C" plus the Export Control

22 FEB 1991

SUBJECT: Technology Screening of Unclassified/Unlimited Reports

Warning Statement. The Controlling DoD Office will mark all other copies of the report with the export control notice specified in DoD Directive 5230.24, Distribution Statements on Technical Documents, to prevent dissemination in a manner that would violate applicable export control laws and regulations.

4. Address responses or questions to DTIC-HAS, telephone (703) 274-6876, DSN 284-6876.

FOR THE ADMINISTRATOR:

Victor Furtado

VICTOR FURTADO
Acting Director, Directorate
of Database Services

DTIC-BAS

22 FEB 1991

SUBJECT: Technology Screening of Unclassified/Unlimited Reports

TO: Commander
U.S. Laboratory Command
Ballistic Research Laboratory
ATTN: SLCBR-DD-T
Aberdeen Proving Ground, MD 21005-5066

1. DTIC has been authorized by DoD to screen and challenge Distribution Statement "A" reports for security and critical technology that should be withheld from public sale through NTIS. Such reports will be available from DTIC only to its registered users.

2. The report referenced below has been received at DTIC and has been screened for security and technology control. The report is believed to contain technical data that should be denied public disclosure according to DoD Directive 5230.25, Withholding of Unclassified Technical Data from Public Disclosure.

Source: Ballistic Research Laboratory
Title: Computation of the Roll Characteristics of the M829 Kinetic Energy Projectile and Comparison with Range Data
Report No. BRL-TR-3172
Date of Report: November 1990

Applicable MCTL Ref.: Page 6-15, Paragraphs 6.4.2.A.1.a. and b.

3. The report will not be released to NTIS or DTIC users until the situation is resolved. Please review the report in accordance with the MCTL reference (cited above). Notify DTIC within 30 days whether the report meets the criteria for public release. If the report has already been exported (released to a foreign national or country), or if there is no response, DTIC will process the report by assigning the Distribution Statement "C": "Distribution limited to U.S. Government Agencies and their Contractors because of Critical Technology (DoD Directive 5230.24)." If the report has not been exported, DTIC will mark the report Statement "C" plus the Export Control

22 FEB 1991

...of Unclassified/Unlimited Reports

...ing ... the controlling DoD office will mark all ... copies of the report with the export control notice specified in DoD directive 5230.24, Distribution Statements on Technical Documents, to prevent dissemination in a manner that would violate applicable export control laws and regulations.

... Address responses or questions to DTIC-HAS, telephone (703) 274-6875, DSN 284-6875.

FOR THE ADMINISTRATOR:

Signed

VICTOR FURTADO
Acting Director, Directorate
of Database Services

NFR: Not necessary
PE: A. Washington/DTIC-HAS/46876/mw/21 Feb 91

COORD:

DTIC-HAS

DTIC-HA

CARES: /dtich/mwhetzel/700.01/challenge5

REPORT DOCUMENTATION PAGE

Form Approved
OMB No. 0704-0188

1. AGENCY USE ONLY (Leave blank)	2. REPORT DATE	3. REPORT TYPE AND DATES COVERED
	November 1990	Final, Sep 88 - Sep 89

4. TITLE AND SUBTITLE

COMPUTATION OF THE ROLL CHARACTERISTICS OF THE M829 KINETIC ENERGY PROJECTILE AND COMPARISON WITH RANGE DATA

5. FUNDING NUMBERS

1L162618AH80
62618A-00-001 AJ

6. AUTHOR(S)

Paul Weinacht and Walter B. Sturek

7. PERFORMING ORGANIZATION NAME(S) AND ADDRESS(ES)

8. PERFORMING ORGANIZATION REPORT NUMBER

9. SPONSORING/MONITORING AGENCY NAME(S) AND ADDRESS(ES)

Ballistic Research Laboratory
ATTN: SLCBR-DD-T
Aberdeen Proving Ground, MD 21005-5066

10. SPONSORING/MONITORING AGENCY REPORT NUMBER

BRL-TR-3172

11. SUPPLEMENTARY NOTES

12a. DISTRIBUTION AVAILABILITY STATEMENT

Approved for public release; distribution is unlimited

12b. DISTRIBUTION CODE

13. ABSTRACT (Maximum 200 words)

A recently developed computational technique has been applied to predict the aerodynamic roll characteristics of the M829 kinetic energy projectile. These aerodynamic parameters include the roll producing moment, the roll damping moment, and the equilibrium spin rate, defined as the spin rate for which the net roll moment is zero. These aerodynamic parameters have been determined by computing the flow field about the projectile using a parabolized Navier-Stokes computational approach. The computations have been performed using a coordinate frame that rotates at the spin rate of the projectile. Comparison is made with results obtained experimentally from range firings and from engineering estimation approaches. The computed equilibrium spin rate and the spin histories agree well with the data obtained from range firings.

14. SUBJECT TERMS

Finned Projectiles, Kinetic Energy Projectiles, Projectile Aerodynamics, Roll Damping, Steady State Spin Rate, Rotating Coordinate Frames, Computational Fluid Dynamics

15. NUMBER OF PAGES

33

16. PRICE CODE

17. SECURITY CLASSIFICATION OF REPORT	18. SECURITY CLASSIFICATION OF THIS PAGE	19. SECURITY CLASSIFICATION OF ABSTRACT	20. LIMITATION OF ABSTRACT
UNCLASSIFIED	UNCLASSIFIED	UNCLASSIFIED	UL

INTENTIONALLY LEFT BLANK.

Table of Contents

INTENTIONALLY LEFT BLANK.

List of Figures

I. INTRODUCTION

The ability to accurately predict the roll characteristics of projectiles is important to the projectile designer. A good kinetic energy (KE) projectile design will have an equilibrium or steady-state spin rate that avoids both the yawing frequency and the projectile's first natural frequency of vibration. The yawing frequency is avoided to preclude the possibility of spin/yaw lock-in. Typically, the natural frequency and the yawing frequency represent an upper and lower bound for the design equilibrium spin rate.

In previous work, a computational approach[1] had been developed and applied to predict the aerodynamic roll characteristics of the M735 KE projectile. These aerodynamic parameters, which include the roll producing moment, the roll damping moment, and the equilibrium spin rate, were determined by computing the flow field about the projectile using a Parabolized Navier-Stokes computational approach. Because no wind tunnel or range tests had been performed to determine the roll characteristic of this projectile, comparisons of the numerical predictions were only made with engineering estimates of these aerodynamic parameters. Further benchmarking of the numerical approach with experimental data was desired.

In this report, the numerical approach has been applied to compute the aerodynamic roll characteristics of the M829 KE projectile. Comparisons are made with data obtained from range firings as well as with engineering predictions of these parameters. A schematic of the M829 projectile is shown in Figures 1 - 4. The particular fin design shown here has roll-producing beveled surfaces at the leading and trailing edge of the fins. Particular care has been taken to model the fin geometry accurately.

In this report, the equation of motion for a projectile undergoing pure rolling motion is briefly discussed in the next section. The computational techniques used to predict the roll characteristics are then presented, followed by a brief discussion of the range data and engineering estimation approach. Presentation and discussion of the results obtained by applying these techniques are then made and, finally, the conclusions of this study are presented.

II. THE ROLL EQUATION

Aero-ballisticians describe the spin history of the projectile in terms of the following ordinary differential equation;[2]

$$I\frac{dp}{dt} = \frac{1}{2}\rho_\infty a_\infty^2 M_\infty^2 D S_{ref} C_l \tag{1}$$

where p is the spin rate, t is time, I is the axial moment of inertia, C_l is the net aerodynamic roll moment coefficient acting on the projectile, and ρ_∞, a_∞, M_∞, D, and S_{ref} are, respectively, the reference density, speed of sound, Mach number, diameter, and area.

The net aerodynamic roll moment is composed of two components, the roll producing moment and the roll damping moment. The roll producing moment, which induces spin

on the projectile, results from the aerodynamic loads produced by either the machined asymmetries in the fin geometry or by the fin cant, while the roll damping contribution consists of pressure and viscous forces that oppose the spin. The relationship of these contributions to the net aerodynamic roll moment is expressed below in non-dimensional form,

$$C_l = C_{l_o} + C_{l_p}\frac{pD}{V} \tag{2}$$

where C_{l_o} is the roll producing moment coefficient, C_{l_p} is the roll damping moment coefficient and $\frac{pD}{V}$ is the non-dimensional spin rate. The roll damping coefficient will differ in sign with the roll producing moment coefficient and will be negative if the direction of positive roll moment is in the direction of positive spin.

In the computational framework where the projectile is flying at constant velocity, Equation 2 shows that the roll producing moment can be obtained by computing the net aerodynamic roll moment at zero spin rate. Likewise, the roll damping moment is obtained by computing the net aerodynamic roll moment on the projectile at a fixed spin rate, subtracting the roll producing moment from it and dividing by the spin rate. The equilibrium spin rate, which occurs when the net aerodynamic roll moment is zero, is obtained by dividing the roll producing moment by the roll damping moment.

A closed form solution[2] of Equation 1 can be obtained by transforming the independent variable from time to distance and by assuming that the aerodynamic coefficients do not vary across the Mach number range of interest. In transforming the independent variable from time to distance, the solution of the drag equation is implicitly included. The solution of this equation is shown below.

$$\frac{pD}{V} = \left(\frac{pD}{V}\right)_0 + \left[\left(\frac{pD}{V}\right)_{ss} - \left(\frac{pD}{V}\right)_0\right](1. - e^{\frac{-K_p s}{D}}) \tag{3}$$

where

$$\begin{aligned} K_p &= -\frac{\rho_\infty S_{ref} D}{2m}\left[C_D + k_a^{-2} C_{l_p}\right] \\ K_\delta &= \frac{\rho_\infty S_{ref} D^3}{2I} C_{l_o} \\ k_a &= \sqrt{\frac{I}{mD^2}} \\ \left(\frac{pD}{V}\right)_{ss} &= \frac{K_\delta}{K_p} \end{aligned} \tag{4}$$

The spin rate at launch, $\left(\frac{pD}{V}\right)_0$, represents an initial condition that must be specified. In the analysis presented here, the spin rate at launch is presumed to be zero. Note that the steady-state spin rate, $\left(\frac{pD}{V}\right)_{ss}$, differs slightly from the equilibrium spin rate defined above in that the drag term appears in the definition of the steady-state spin rate. For the case of zero drag (projectile is flying at constant velocity), the steady-state spin rate becomes identical to the equilibrium spin rate. The difference between the equilibrium spin rate and the steady-state spin rate is about one half of one percent for the projectile examined here.

III. COMPUTATIONAL APPROACH

Computation of the viscous flow field about the finned projectile configuration was accomplished by solving the thin-layer Navier-Stokes equations using a parabolized Navier-Stokes technique. The computations have been performed in a coordinate frame that rotates at the spin rate of the projectile. The fluid flow relative to the rotating coordinate frame does not vary with time, allowing the steady (non-time varying) Navier-Stokes equations to be applied. The solution of the steady Navier-Stokes equations can be performed at a reasonable computational cost. In order to implement the rolling coordinate frame, the governing equations have been modified to include the effects of centrifugal and Coriolis forces. The steady thin-layer Navier-Stokes equations are shown below.

$$\frac{\partial \hat{E}}{\partial \xi} + \frac{\partial \hat{F}}{\partial \eta} + \frac{\partial \hat{G}}{\partial \zeta} + \hat{H}_c + \hat{H} = \frac{1}{Re}\left(\frac{\partial \hat{S}}{\partial \zeta} + \hat{S}_c\right) \tag{5}$$

Here, $\hat{E}$, $\hat{F}$, and $\hat{G}$ are the inviscid flux vectors, $\hat{S}$ is the viscous flux vector, $\hat{H}_c$ and $\hat{S}_c$ are inviscid and viscous source terms due to the cylindrical coordinate formulation, and $\hat{H}$ is the source term containing the Coriolis and centrifugal force terms which result from the rotating coordinate frame. Each of these matrices are functions of the dependent variables represented by the vector $q(\rho, \rho u, \rho v, \rho w, e)$, where ρ and e are the density and the total energy per unit volume, and u, v, and w, are the velocity components in axial, circumferential, and normal directions. The flux terms are shown below.

$$\hat{E} = \frac{1}{J}\begin{bmatrix} \rho U \\ \rho u U + \xi_x p \\ \rho v U \\ \rho w U \\ (e+p)U \end{bmatrix} \qquad \hat{F} = \frac{1}{J}\begin{bmatrix} \rho V \\ \rho u V + \eta_x p \\ \rho v V + \eta_\theta p/r \\ \rho w V + \eta_r p \\ (e+p)V \end{bmatrix}$$

$$\hat{G} = \frac{1}{J}\begin{bmatrix} \rho W \\ \rho u W + \zeta_x p \\ \rho v W + \zeta_\theta p/r \\ \rho w W + \zeta_r p \\ (e+p)W \end{bmatrix} \qquad \hat{H}_c = \frac{1}{Jr}\begin{bmatrix} \rho w \\ \rho u w \\ 2\rho v w \\ \rho(w^2 - v^2) \\ (e+p)w \end{bmatrix} \tag{6}$$

$$\hat{S} = \frac{1}{J}\begin{bmatrix} 0 \\ m_1 \dfrac{\partial u}{\partial \zeta} + m_2 \zeta_x \\ m_1 \dfrac{\partial v}{\partial \zeta} + m_2 \zeta_\theta / r \\ m_1 \dfrac{\partial w}{\partial \zeta} + m_2 \zeta_r \\ m_3 \end{bmatrix} \qquad \hat{H} = \frac{1}{J}\begin{bmatrix} 0 \\ 0 \\ 2\Omega\rho w \\ -2\Omega\rho v - \Omega^2 r \rho \\ -\Omega^2 r \rho w \end{bmatrix}$$

$$\hat{S}_c = \frac{1}{J}\begin{bmatrix}
0 \\
-\zeta_x\frac{\partial}{\partial\zeta}\left((\mu+\mu_t)\frac{2w}{3r}\right)+\frac{\mu+\mu_t}{r}\left(\zeta_r\frac{\partial u}{\partial\zeta}+\zeta_x\frac{\partial w}{\partial\zeta}\right) \\
-\zeta_r\frac{\partial}{\partial\zeta}\left((\mu+\mu_t)\frac{v}{r}\right)+\frac{\zeta_\theta}{r}\frac{\partial}{\partial\zeta}\left((\mu+\mu_t)\frac{4w}{3r}\right) \\
\quad+\frac{2(\mu+\mu_t)}{r}\left(\frac{\zeta_\theta}{r}\frac{\partial w}{\partial\zeta}+\zeta_r\frac{\partial v}{\partial\zeta}-\frac{v}{r}\right) \\
-\frac{\zeta_\theta}{r}\frac{\partial}{\partial\zeta}\left((\mu+\mu_t)\frac{v}{r}\right)-\zeta_r\frac{\partial}{\partial\zeta}\left((\mu+\mu_t)\frac{2w}{3r}\right) \\
\quad+\frac{2(\mu+\mu_t)}{r}\left(\frac{-\zeta_\theta}{r}\frac{\partial v}{\partial\zeta}+\zeta_r\frac{\partial w}{\partial\zeta}-\frac{w}{r}\right) \\
-\zeta_x\frac{\partial}{\partial\zeta}\left((\mu+\mu_t)\frac{2uw}{3r}\right)+\frac{\zeta_\theta}{r}\frac{\partial}{\partial\zeta}\left((\mu+\mu_t)\frac{vw}{3r}\right) \\
\quad-\frac{\zeta_r}{r}\frac{\partial}{\partial\zeta}\left((\mu+\mu_t)\left(v^2+\frac{2}{3}w^2\right)\right)+\frac{(\mu+\mu_t)\zeta_r}{2r}\frac{\partial}{\partial\zeta}\left(q^2\right) \\
\quad-\frac{2w(\mu+\mu_t)}{3r}\left(\zeta_x\frac{\partial u}{\partial\zeta}+\frac{\zeta_\theta}{r}\frac{\partial v}{\partial\zeta}+\zeta_r\frac{\partial w}{\partial\zeta}\right) \\
\quad+\frac{(\mu+\mu_t)}{r}\left(u\zeta_x\frac{\partial w}{\partial\zeta}+\frac{v\zeta_\theta}{r}\frac{\partial w}{\partial\zeta}+w\zeta_r\frac{\partial w}{\partial\zeta}\right) \\
\quad+\frac{1}{\gamma-1}\left(\frac{\mu}{Pr}+\frac{\mu_t}{Pr_t}\right)\zeta_r\frac{\partial}{\partial\zeta}\left(a^2\right)
\end{bmatrix} \tag{7}$$

where

$$\begin{aligned}
U &= u\xi_x \\
V &= u\eta_x + v\eta_\theta/r + w\eta_r \\
W &= u\zeta_x + v\zeta_\theta/r + w\zeta_r
\end{aligned} \tag{8}$$

$$\begin{aligned}
m_1 &= (\mu+\mu_t)(\zeta_x^2+(\zeta_\theta/r)^2+\zeta_r^2) \\
m_2 &= \frac{1}{3}(\mu+\mu_t)(\zeta_x\frac{\partial u}{\partial\zeta}+\frac{1}{r}\zeta_\theta\frac{\partial v}{\partial\zeta}+\zeta_r\frac{\partial w}{\partial\zeta}) \\
m_3 &= \frac{1}{(\gamma-1)}(\frac{\mu}{Pr}+\frac{\mu_t}{Pr_t})(\zeta_x^2+(\zeta_\theta/r)^2+\zeta_r^2)\frac{\partial a^2}{\partial\zeta}+\frac{1}{2}m_1\frac{\partial q^2}{\partial\zeta} \\
&\quad +m_2(u\zeta_x+\frac{v}{r}\zeta_\theta+w\zeta_r)
\end{aligned} \tag{9}$$

$$a^2 = \frac{\gamma p}{\rho} \tag{10}$$

$$q^2 = u^2+v^2+w^2 \tag{11}$$

$$
\begin{array}{lll}
\xi_x = \frac{1}{x_\xi} & & \\
\eta_x = J(r_\xi \theta_\zeta - \theta_\xi r_\zeta) & \eta_\theta = J(x_\xi r_\zeta) & \eta_r = J(-x_\xi \theta_\zeta) \\
\zeta_x = J(\theta_\xi r_\eta - r_\xi \theta_\eta) & \zeta_\theta = J(-x_\xi r_\eta) & \zeta_r = J(x_\zeta \theta_\eta) \\
J = 1/\left(x_\xi \left(\theta_\eta r_\zeta - \theta_\zeta r_\eta\right)\right) & &
\end{array} \tag{12}
$$

The pressure, p, can be related to the dependent variables by applying the ideal gas law.

$$
p = (\gamma - 1)\left[e - \frac{\rho}{2} q^2\right] \tag{13}
$$

The thin-layer equations are solved using the Parabolized Navier-Stokes technique of Schiff and Steger.[3] Following the approach of Schiff and Steger, the governing equations, which have been modified here to include the Coriolis and centrifugal force terms, are solved using a conservative, approximately factored, implicit finite-difference numerical algorithm as formulated by Beam and Warming.[4]

Following the approach of Schiff and Steger, the equations are first linearized and placed in delta form, where the equations are solved for the difference in the dependent variables rather than the variable itself. This set of equations is then factorized using the approach of Beam and Warming. The following set of equations is obtained.

$$
\left[\tilde{A}_s^j + (1-\alpha)\Delta\xi\left(\delta_\eta \tilde{B}^j + \tilde{D}^j + \tilde{D}_c{}^j\right)\right]\Delta\hat{q}^* = RHS \tag{14}
$$

$$
\left[\tilde{A}^j + (1-\alpha)\Delta\xi\left(\delta_\zeta \tilde{C}^j - \frac{1}{Re}\left(\bar{\delta}_\zeta \tilde{M}^j + \tilde{M}_c{}^j\right)\right)\right]\Delta\hat{q}^j = \tilde{A}_s^j \Delta\hat{q}^* \tag{15}
$$

$$
\begin{aligned}
RHS \;=\; & -(\tilde{A}_s^j - \tilde{A}_s^{j-1})\hat{q}^j + \alpha(\hat{E}_s^j - \hat{E}_s^{j-1}) - \left[(\xi_x/J)^{j+1} E_p^j - (\xi_x/J)^j E_p^{j-1}\right] \\
& -(1-\alpha)\Delta\xi\{\delta_\eta\left[\eta_x^{j+1}(E/J)^j + (\eta_\theta/r)^{j+1}(F/J)^j + \eta_r^{j+1}(G/J)^j\right] \\
& +\delta_\zeta\left[\zeta_x^{j+1}(E/J)^j + (\zeta_\theta/r)^{j+1}(F/J)^j + \zeta_r^{j+1}(G/J)^j\right] \\
& +\hat{H}^j + \hat{H}_c^j - \frac{1}{Re}\left(\bar{\delta}_\zeta \tilde{S}^j + \tilde{S}_c{}^j\right)\}
\end{aligned} \tag{16}
$$

The form of the equations, as well as the notation, is similar to that used by Schiff and Steger. Here, $\tilde{A}$, $\tilde{B}$, $\tilde{C}$, and $\tilde{M}$ are the Jacobian matrices of the flux vectors $\hat{E}$, $\hat{F}$, $\hat{G}$, and $\hat{S}$. Further details on the definitions of these matrices can be found in Reference 3. The important difference here is the addition of the matrices $\tilde{D}$ and $\hat{H}$ due to the rotating coordinate system. Although the Jacobian matrix, $\tilde{D}$, can be included in either the circumferential inversion or the normal inversion, including this term in the circumferential inversion simplifies slightly the implementation of the shock fitting boundary conditions.

Two additional Jacobian matrices, $\tilde{D}_c$ and $\tilde{M}_c$, appear in these equations and are due to the linearization of the inviscid and viscous cylindrical coordinate source terms; $\hat{H}_c$ and $\hat{S}_c$. The addition of the Jacobian matrices due to the cylindrical coordinate terms has been performed during the course of this study and represents an improvement in the formulation. Numerical experiments have shown, however, that the implicit treatment of these terms has little affect on the computed flow field for the cases examined here.

The computations presented here were performed using a shock fitting procedure reported by Rai and Chaussee.[5] This procedure solves the five Rankine-Hugoniot jump conditions, two geometric shock-propagation conditions, and one compatibility equation to determine the values of the five dependent variables immediately behind the shock, as well as the position of the shock. By including the implicit part of the source term due to the rotating coordinate frame in the circumferential inversion, the shock fitting procedure of Rai and Chaussee can be used without modification, as long as the correct free-stream conditions are specified as shown below in non-dimensional form.

$$\begin{aligned} \rho &= 1. \\ \rho u &= M_\infty \\ \rho v &= r\Omega \\ \rho w &= 0. \\ e &= 1./\gamma(\gamma-1) + \frac{1}{2}\{M_\infty^2 + r^2\Omega^2\} \end{aligned} \tag{17}$$

The computational results presented here were obtained using a grid that consisted of 60 points between the body and the shock. In the circumferential direction, gridding was performed over a 60 degree sector due to the periodic symmetry present in the configuration examined here. Over the forebody, six circumferential points were used, though the flow here is axisymmetric. On the finned portion of the body, 50 points were used in the circumferential direction. The grid over this part of the body was generated using an elliptic grid generation scheme presented by Rai and Chaussee.[6]

The computations were performed using a Cray-2 supercomputer. Solutions over the axisymmetric and finned portion of the body were obtained in 250 seconds and 1100 seconds respectively.

The turbulent viscosity, μ_t, which appears in the viscous matrices, was computed using the Baldwin-Lomax turbulence model.[7]

IV. ENGINEERING ESTIMATION APPROACH

Two simple approaches have been formulated to estimate the roll producing and roll damping moments, and subsequently, the equilibrium spin rate. These approaches are typical of the approaches currently adopted by some projectile designers.

1. Estimation of the Roll Damping of a KE Fin

One approach for estimating the roll damping of a KE fin is to use a strip theory approach; a technique that divides the fin planform into many small chord-wise strips. Each strip is assumed to be a two-dimensional flat plate at angle of attack, where the local angle of attack is a function of the local circumferential velocity due to the spin and the axial component of the velocity. The roll moment is then determined by integrating the lift on each strip multiplied by the local moment arm. Note that the sign of the roll moment

will be negative since the roll moment opposes the spin. The roll damping moment, which is the variation in the roll moment with spin, can be determined by dividing the roll moment by the non-dimensional spin rate, since roll producing moment on the flat plate fin will be zero. In the current approach, the lift on each strip is determined from linearized potential theory. The resulting equation for the roll damping moment coefficient is shown below,

$$C_{l_p} = \frac{-16N_{fins}}{\pi\sqrt{M_\infty^2 - 1}} \int_{r_{root}/D}^{r_{tip}/D} \frac{c(r/D)}{D} \left(\frac{r}{D}\right)^2 d\left(\frac{r}{D}\right) \tag{18}$$

where N_{fins} is the number of fins, $c(r/D)$ is the local chord length at the nondimensional radial position r/D, and r_{root} and r_{tip} are the radial locations of the fin root and fin tip.

2. Estimation of the Roll Producing Moment on a Beveled Fin

The roll producing moment caused by the machined asymmetries on the leading and trailing edges of the fin can be estimated using an approach similar to that applied to estimate the roll damping moment. Strip theory is again applied, and the fin is treated as a two-dimensional flat plate at angle of attack, where the local angle of attack is equal to the local cant angle, $\delta(\frac{r}{D})$. The cant angle of the fin is produced by the deflection of the leading and trailing edges of the fins due to the beveling. The cant angle is shown schematically in Figure 5. The roll producing moment is determined by integrating the lift on each strip multiplied by the local moment arm. As before, the lift on each strip is determined from linearized potential theory. The resulting integral expression for the roll producing moment coefficient is shown below.

$$C_{l_o} = \frac{16N_{fins}}{\pi\sqrt{M_\infty^2 - 1}} \int_{r_{root}/D}^{r_{tip}/D} \frac{c(r/D)\delta(r/D)}{D} \left(\frac{r}{D}\right) d\left(\frac{r}{D}\right) \tag{19}$$

V. RANGE RESULTS

During 1983, eleven M829 rounds were fired through the Ballistic Research Laboratory Transonic Range.[8] The launch Mach number of the rounds varied between 3.50 and 5.27, as shown in Table 1. Because of restrictions on firing depleted uranium through the Transonic Range, the rounds were modified by replacing the depleted uranium core with a steel core. The external shape of the projectile was not changed, thus the aerodynamics of the rounds fired through the range should be identical to the fielded round. The inflight motion of the rounds was measured, including the spin rate at two stations along the trajectory. Spin rates were measured using spin card arrays. A tabulation of the measured spin rates is shown in Table 1.

Using the closed form solution of the roll equation (Equation 3), a curve fit was performed through the measured spin history for each of the rounds. Since rounds fired from a smooth-bore gun typically have nearly zero initial spin rate, the initial spin rate was assumed to be zero. With the initial spin rate specified, the roll equation contains two additional parameters, K_p and ϕ_{ss}, that were fit uniquely using the spin data obtained at

the two measurement stations. The roll producing and roll damping moment coefficients were then extracted from these parameters using Equation 4. The drag coefficient used in extracting the roll damping moment coefficient was obtained from the range reduction.[8] The steady-state spin rate, roll producing moment coefficient, and roll damping moment coefficient obtained from the reduction are also shown in Table 1.

VI. RESULTS

Computations have been performed to predict the following aerodynamic parameters that determine the roll characteristics of the M829 projectile: the roll producing moment, the roll damping moment, and the equilibrium spin rate. The computations were performed over a range of Mach numbers (M = 3.0 to 5.5) and non-dimensional spin rates (pD/V = 0.0 to 0.015) for free-flight, sea-level atmospheric conditions.

Particular care has been taken to model the fin geometry accurately, including the roll-producing beveled surfaces at the leading and trailing edge of the fins. It should also be noted that the fins on this projectile overhang the base. This aspect of the projectile was modeled by extending the base so that it was aligned with the trailing edge of the fins. This allowed the flow field to be computed up to the trailing edge of the fins. However, when the pressure and viscous stresses were integrated to compute the forces acting on the body, the contribution from this part of the body was not considered. Because the flow is supersonic and the fins are not immersed in the recirculating flow in the base region, the flow field adjacent to this region can be considered to be reasonably well modeled. Though not shown, the cylindrical portion of the body has a number of circumferential grooves which cover nearly two-thirds of the body. The effect of these grooves is not modeled in the current computations, though it is a subject of current research.

The computed roll characteristics were compared with values determined from engineering estimation approaches and with results obtained from range firings. Roll histories were obtained by solving the roll equation using the computed aerodynamic roll moment coefficients and were compared with the range measurements. In this section, the computational results are first presented independently, followed by discussion of comparisons of the computational results with the engineering approach and range results.

1. Computational Results

The roll producing moment is obtained by computing the net roll moment at zero spin rate. Figure 6 shows the development of the roll producing moment coefficient as it is integrated down the body at Mach 4. The roll producing moment initially shows rapid increase over the front of the fin due to the leading edge bevel. At axial locations near the aft end of the leading edge bevel (and upstream of the trailing edge bevel), the roll moment decreases somewhat due to a pressure differential across the fin which opposes the roll moment component from the leading edge bevel. The roll moment begins to increase again at axial locations where the trailing edge bevel exists.

Figure 7 shows the pressure distribution on both sides of the fin at a spanwise location that is half-way between the root and tip chords. This pressure profile is typical of other spanwise locations. The roll producing pressure differentials from the leading and trailing edge bevels are evident, as well as the opposing pressure differential between the two bevels.

The computed roll producing moment as a function of Mach number is shown in Figure 8. The computed results show that the roll producing moment has a maximum value at Mach 4. The decrease in the roll producing moment below Mach 4 is due to the increasing role of the pressure differential downstream of the leading edge bevel which opposes the roll producing contributions from the leading and trailing edge bevels.

The development of the net roll moment acting on the body at non-dimensional spin rates of zero and 0.0074 is shown in Figure 9. The difference between these two curves is the roll damping contribution to the net roll moment. This difference is also shown in this figure. The magnitude of the roll damping contribution shows a rapid increase over the swept portion of the fin. On the aft portion of the fin, where the fin has reached its maximum span, the roll damping contribution does not increase as rapidly. This is due in part to tip effects, which become more pronounced at the lower Mach numbers considered here.

The variation of the net roll moment with spin rate at Mach 4 is shown in Figure 10. For the range of spin rates of interest in the current study, the net roll moment exhibits a linear variation with spin rate. The slope of this curve represents the roll damping moment coefficient, since the roll damping moment is, by definition, the variation of net roll moment with spin rate. The variation of the roll damping moment coefficient with Mach number is seen in Figure 11. The magnitude of the roll damping moment coefficient has a maximum at about Mach 3.5. The roll damping decreases somewhat below Mach 3.5, due to tip effects.

Figure 10 also shows that at Mach 4, the net roll moment is zero at a non-dimensional spin rate 0.0091. This spin rate is the equilibrium spin rate, since the roll producing moment is balanced by the roll damping moment. The variation of the equilibrium spin rate with Mach number is shown in Figure 12. Above Mach 4, the equilibrium spin rate shows little variation with Mach number. At lower Mach numbers, the equilibrium spin rate shows a slight decrease with decreasing Mach number, because the roll producing moment coefficient is decreasing faster than the roll damping moment coefficient.

2. Computational and Engineering Approach Results

A comparison of the predictions of the computational approach and the engineering estimation approach has been performed. Figures 13-15 show the roll producing moment coefficient, the roll damping moment coefficient, and the equilibrium spin rate obtained using the computational and engineering estimation approaches.

The engineering estimates of the roll producing and roll damping moment coefficient both show an asymptotic behavior with Mach number. When compared to the computational results, these estimates show a significant over-prediction of greater than 100 percent

for both these coefficients at Mach 3, though the over-prediction in the vicinity of a typical launch Mach number (Mach 5) is reduced to about 25 percent.

The engineering estimates of the equilibrium spin rate is within 15 percent of the computed results. The engineering estimate of the equilibrium spin rate is independent of Mach number, though the computed results show a variation of over 20 percent across the Mach number regime.

3. Comparison with Range Results

Using the computed roll producing and roll damping moment coefficients, spin histories of the projectile were determined by solving the roll equation (Equation 3). Spin trajectories were obtained for four launch Mach numbers; 3.5, 4.0, 4.65, and 5.25; corresponding closely to the four groups of launch Mach numbers used in the range firings. These trajectories are shown in Figures 16-19. The computed spin histories fall within the range of the range data at both of the measurement locations. The computed trajectories show that at the second measurement station, the projectile is within 3 percent of the steady-state spin rate.

As was discussed in Section V, the steady-state spin rate and the roll producing and roll damping moment coefficients were determined from the range measurements. The comparison between range and computed values of these parameters is made in the next several figures.

Figure 20 shows the comparison of the steady-state spin rate as a function of Mach number. The computed results are bracketed by the range data, demonstrating that the predictions of the steady-state spin rate are within the accuracy of measurements.

Comparisons of the roll producing and roll damping moment coefficients are shown in Figures 21 and 22. The computed results for both coefficients lie somewhat above the range data. At Mach 5.25, the range values of the roll producing moment coefficient are 4 to 35 percent below the computed result, while the range values of the roll damping moment coefficient are 10 to 38 percent below the computed value. The result that both coefficients show similar comparisons between range and computed values is a reflection of the fact that the steady-state spin rate is approximately the ratio of the roll producing moment coefficient to the roll damping moment coefficient. As was shown in Figure 20, this ratio is accurately predicted.

It has been noted by other investigators[8] that some of the round-to-round variability in the spin history of the projectile can be traced to variability in the fin geometry (particularly the beveled surfaces) which occur during manufacturing. These variations should primarily impact the roll producing moment coefficient. However, this does not appear to be a significant factor in the range results examined in this report, because similar variations are seen in both the roll producing and roll damping moment coefficients.

Some of the variability in the range values of roll producing and roll damping moment coefficient can be traced to the measurement of the spin rate at the two measurement stations. For example, it can be shown that a ± 10 percent variation in the roll rate at

the first measurement location will result in about a ±20 percent variation in the roll producing or roll damping moment coefficients. Improvements in the determination of the roll coefficients can be made by increasing the number of measurement stations.

VII. CONCLUSION

The roll characteristics of the M829 kinetic energy projectile have been determined using a recently developed Computational Fluid Dynamics (CFD) approach. The computed roll characteristics, as well as predicted spin histories, have been compared with results obtained using engineering estimation approaches and with data obtained from range firings.

The computed steady-state roll rate and the spin histories agree well with the values obtained from range firings. The predicted roll producing moment and roll damping moment coefficients lie somewhat above most of the range data, though the range data does show considerable scatter. Further validation of the computed roll moment coefficients is desirable. However, this will require improving the determination of these coefficients from the range firings, perhaps by using additional measurement stations.

Equilibrium spin rate predictions made with an engineering estimation approach are within fifteen percent of the computational predictions. The engineering estimates of the roll producing and roll damping moment coefficients showed substantial over-predictions compared with the computational results, though the results near the launch Mach number were within 25 percent.

Table 1. Range Measurements of Roll Trajectories

Round Number	Mach Number	Spin Rate 71 Meters from the Gun (pD/V)	Spin Rate 256 Meters from the Gun (pD/V)	Steady State Roll Rate (pD/V)	Roll Producing Moment Coefficient	Roll Damping Moment Coefficient
23439	5.27	0.00511	0.00802	0.00827	0.0893	10.86
23440	5.25	0.00639	0.01034	0.01075	0.1089	10.19
23441	5.26	0.00525	0.00918	0.00978	0.0845	8.70
23442	4.64	0.00558	0.00813	0.00828	0.1041	12.65
23443	4.64	0.00496	0.00825	0.00865	0.0827	9.63
23551	3.98	0.00620	0.00953	0.00979	0.1102	11.34
23562	4.02	0.00658	0.01150	0.01226	0.1060	8.73
23563	3.50	0.00581	0.00999	0.01059	0.0946	9.02
23564	3.53	0.00744	0.00972	0.00978	0.1569	16.14
23575	3.57	0.00504	0.00914	0.00989	0.0790	8.07
23576	4.67	0.00558	0.00872	0.00898	0.0978	10.96

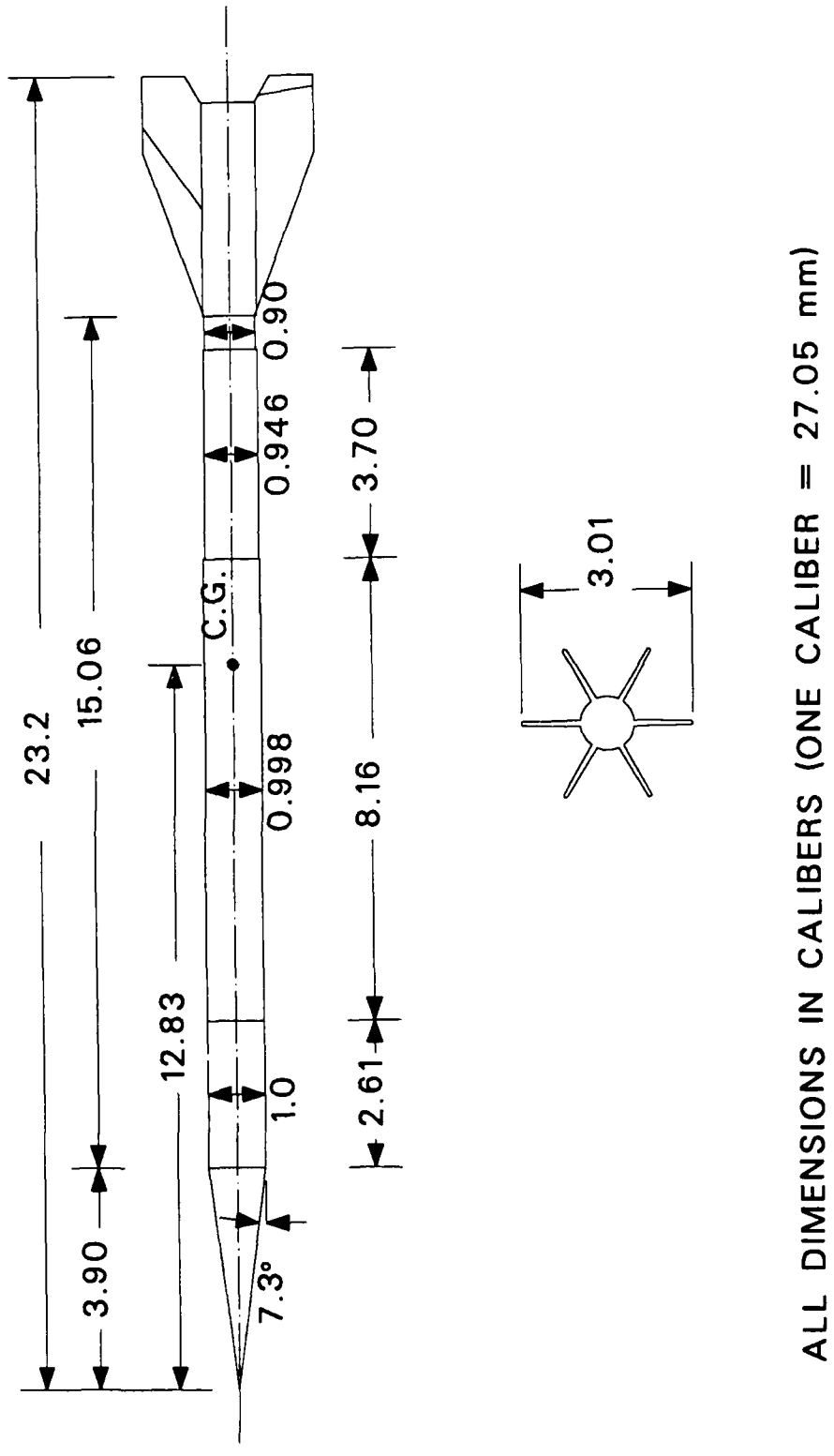

Figure 1. Schematic of M829 projectile

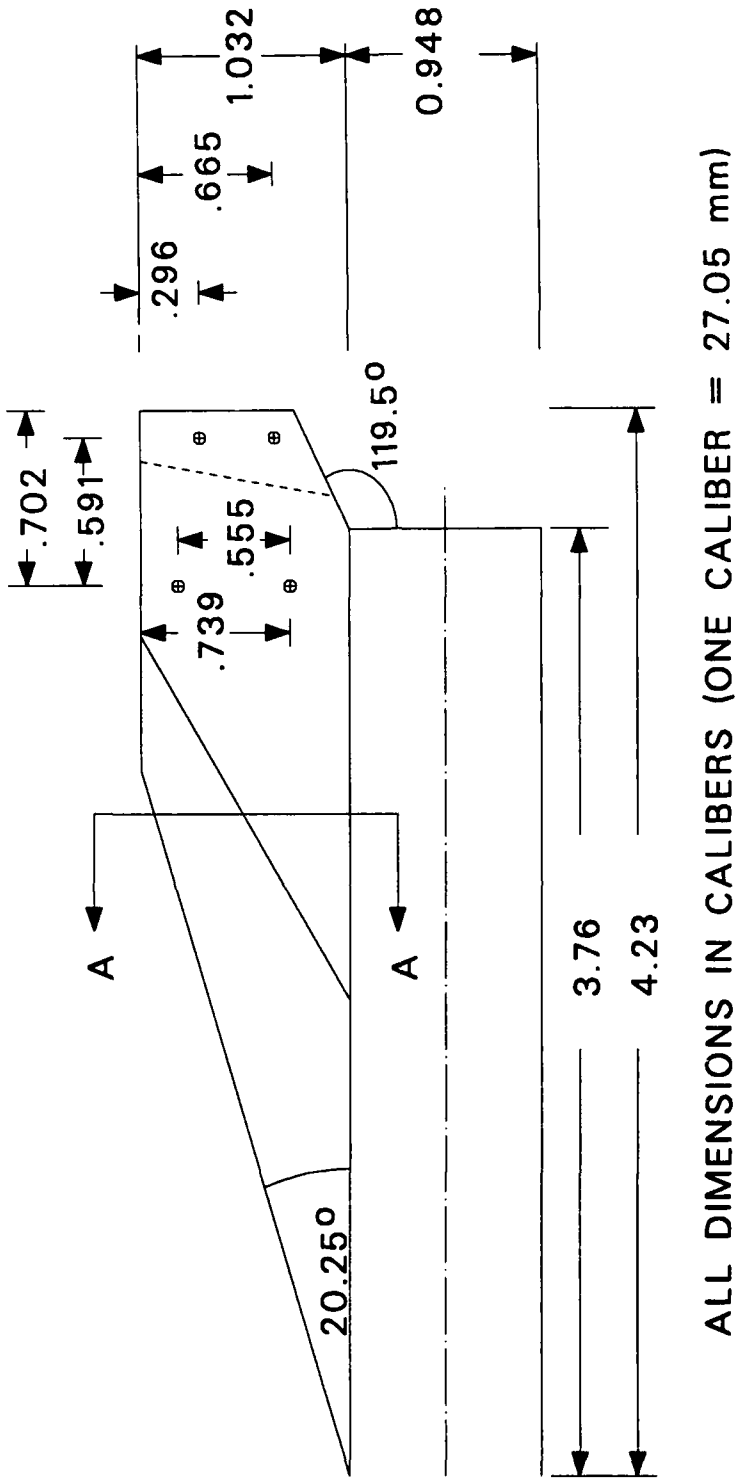

Figure 2. Schematic of M829 fin

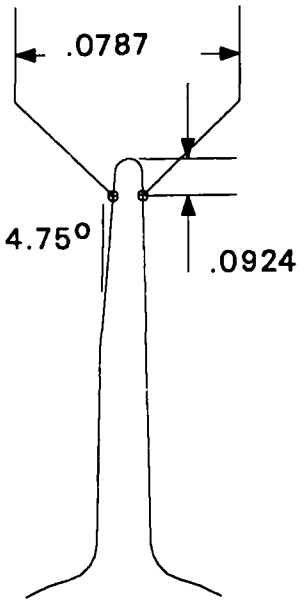

Figure 3. Detail of M829 leading edge

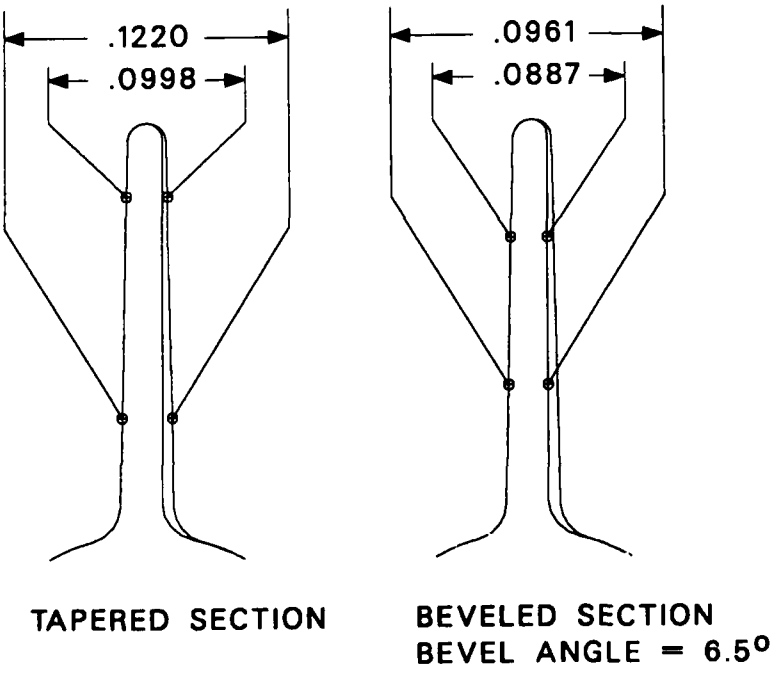

Figure 4. Detail of M829 trailing edge

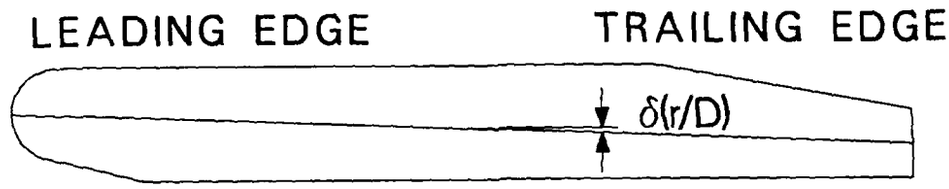

Figure 5. Cross-sectional view of fin showing cant angle

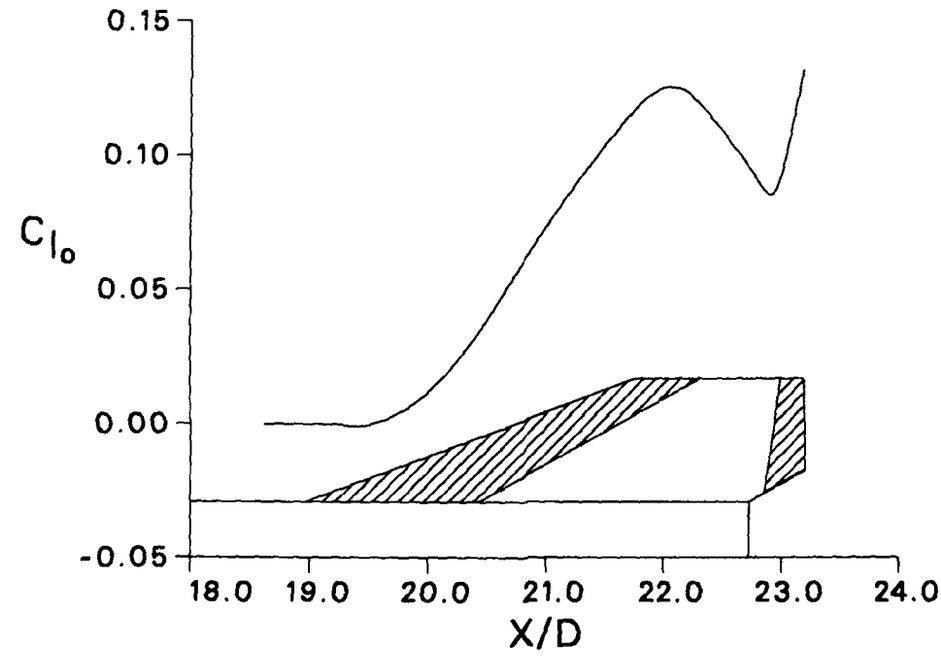

Figure 6. Development of roll producing moment coefficient over fins, Mach = 4

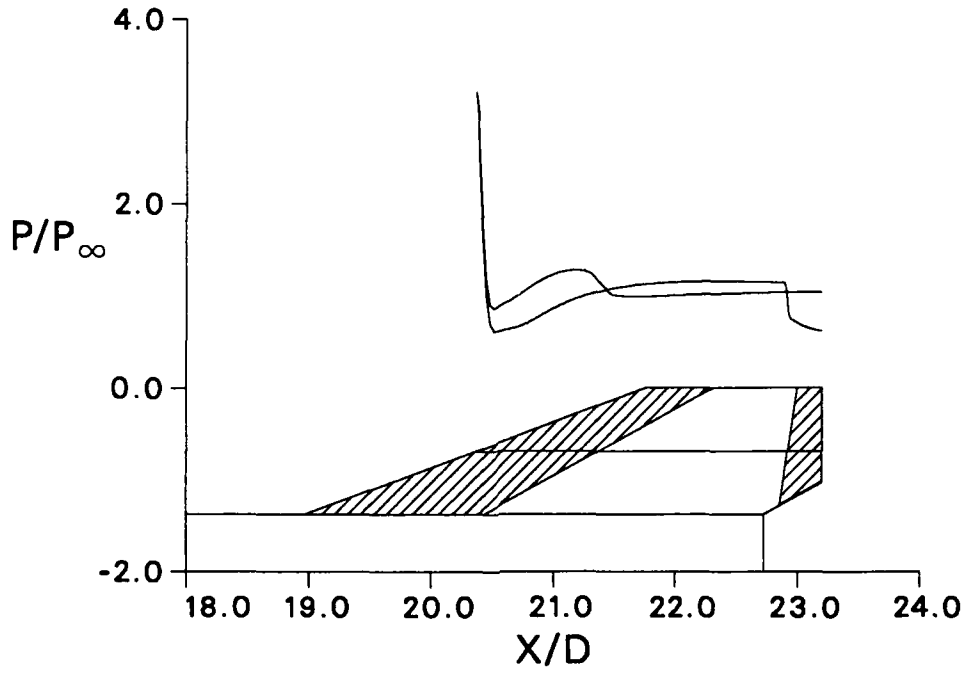

Figure 7. Pressure distribution on fin at mid-span, Mach 4

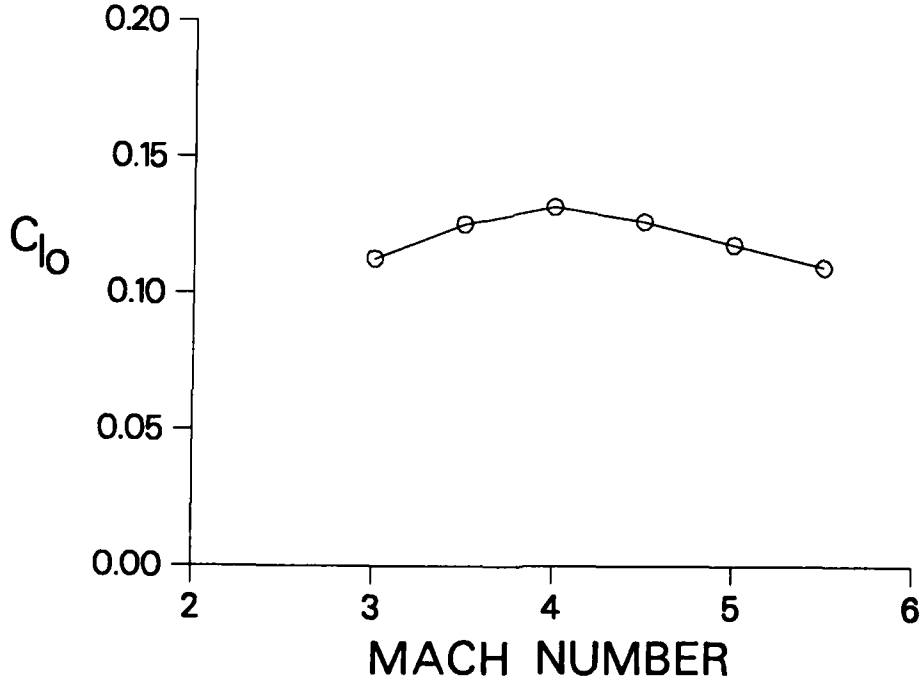

Figure 8. Variation of computed roll producing moment coefficient with Mach number

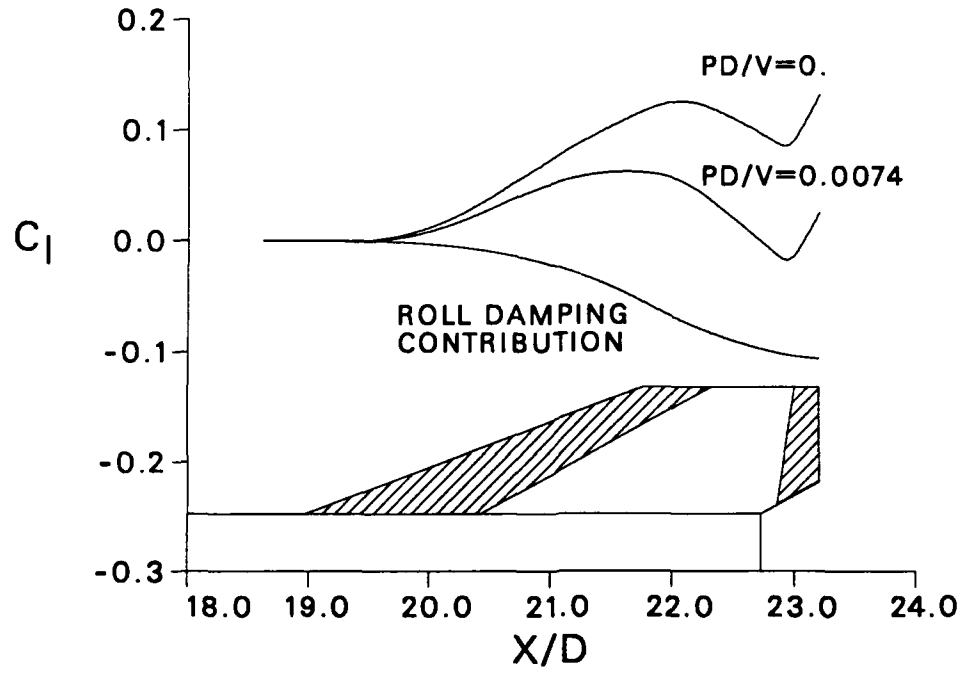

Figure 9. Development of net roll moment coefficient over fins, Mach 4

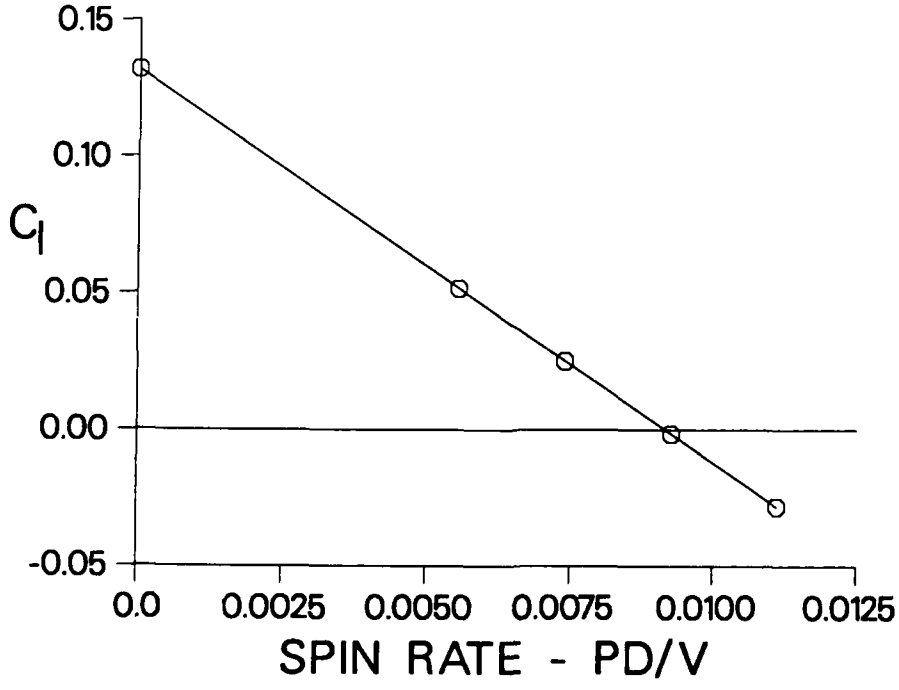

Figure 10. Variation of net roll moment coefficient with spin rate, Mach 4

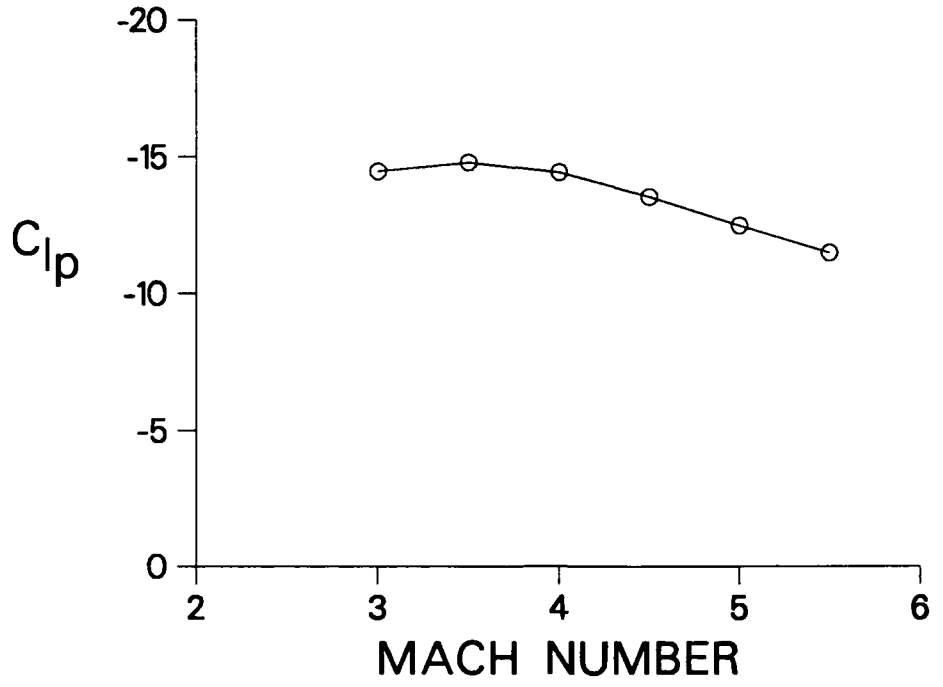

Figure 11. Variation of computed roll damping moment coefficient with Mach number

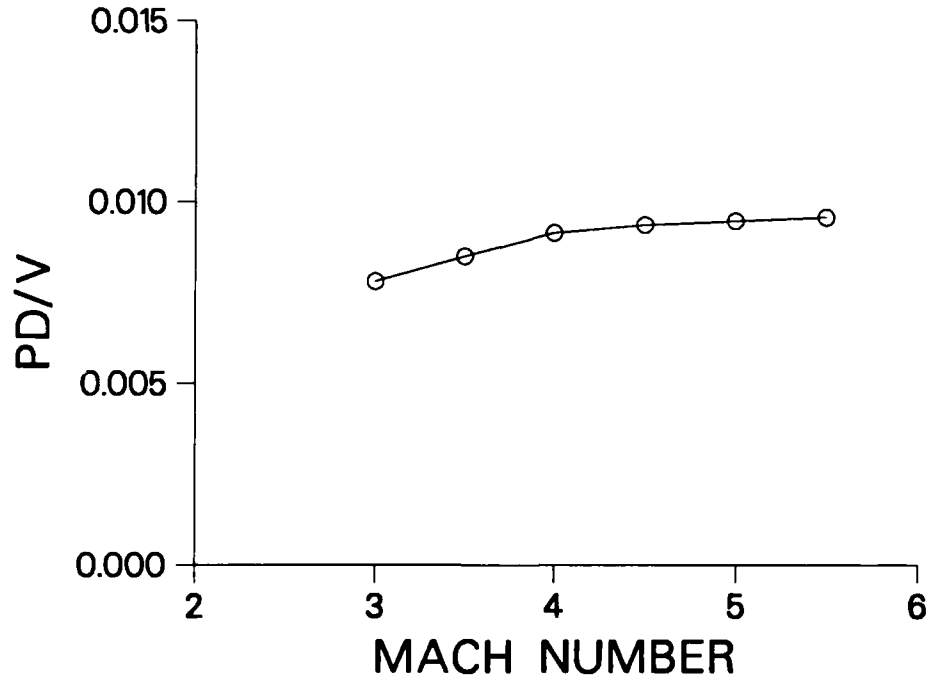

Figure 12. Variation of computed equilibrium spin rate with Mach number

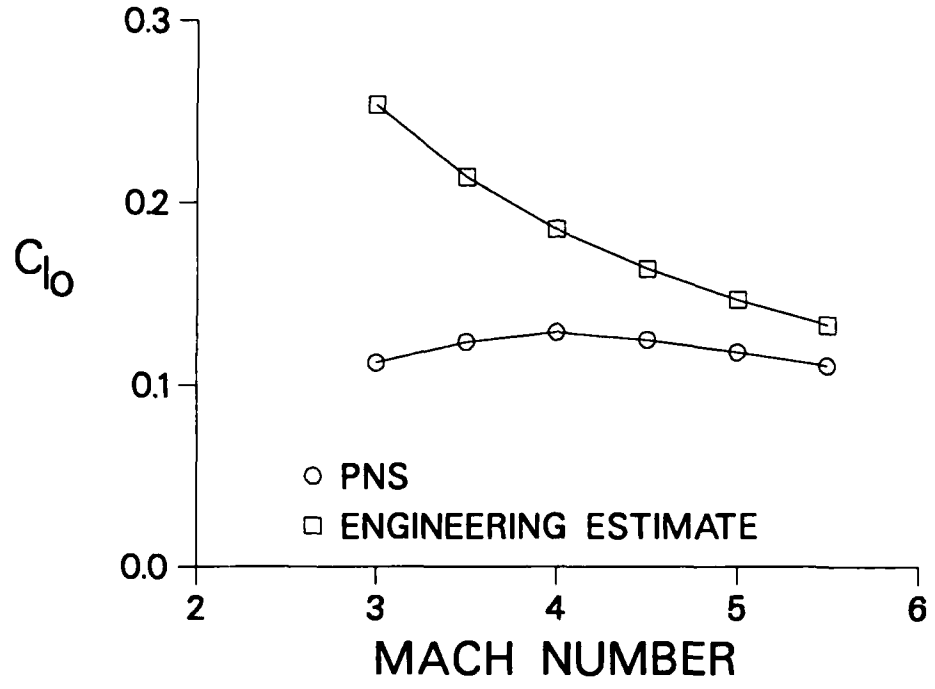

Figure 13. Variation of engineering and computed predictions of roll producing moment coefficient with Mach number

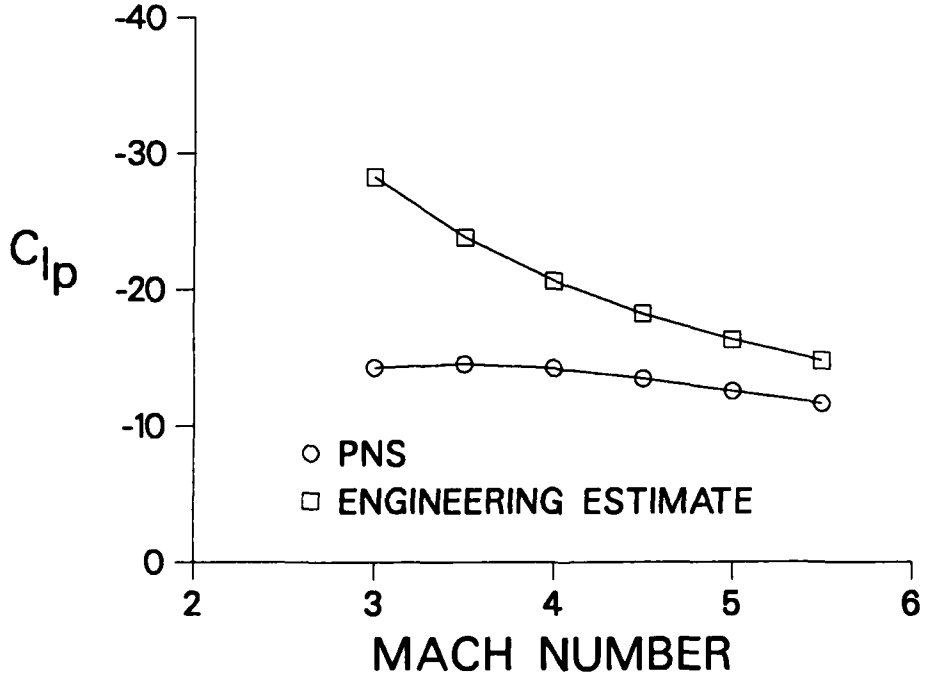

Figure 14. Variation of engineering and computed predictions of roll damping moment coefficient with Mach number

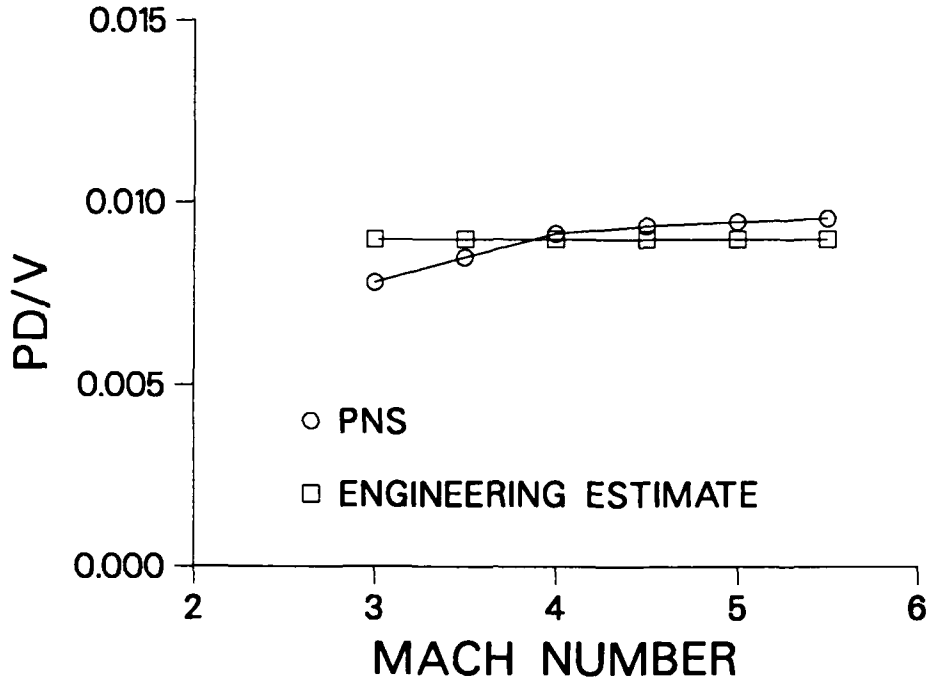

Figure 15. Variation of engineering and computed predictions of equilibrium spin rate with Mach number

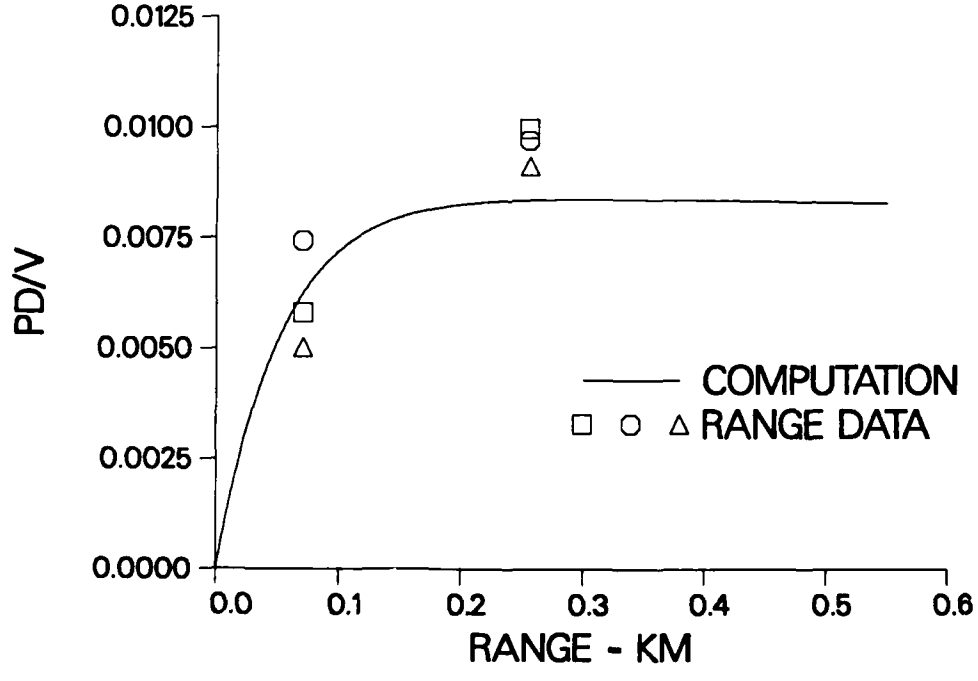

Figure 16. Comparison computed roll history with range data - Launch Mach number = 3.50

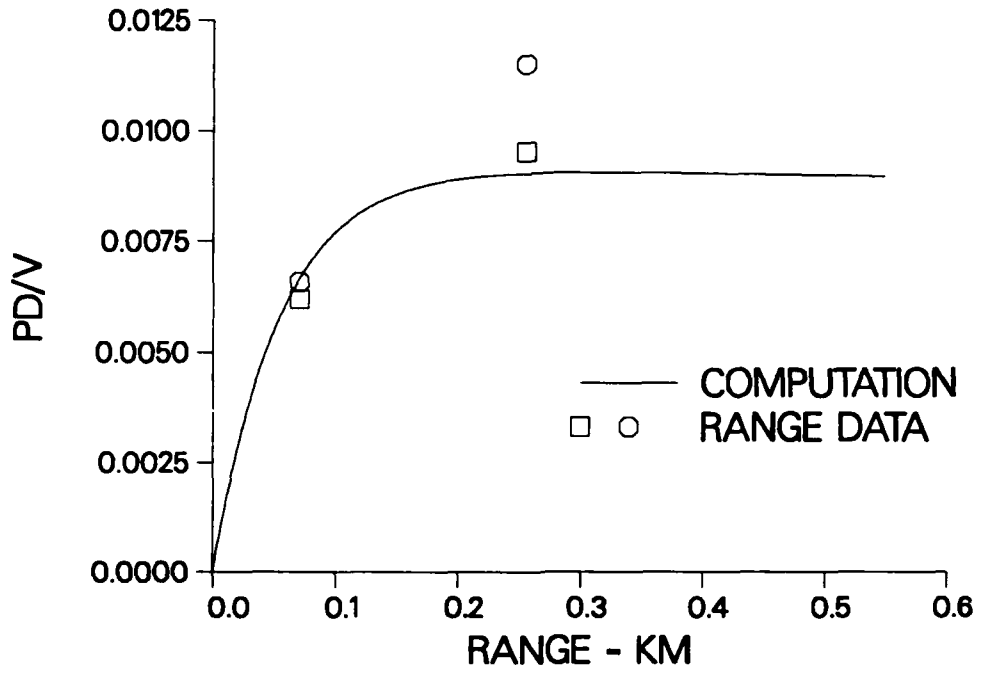

Figure 17. Comparison computed roll history with range data - Launch Mach number = 4.00

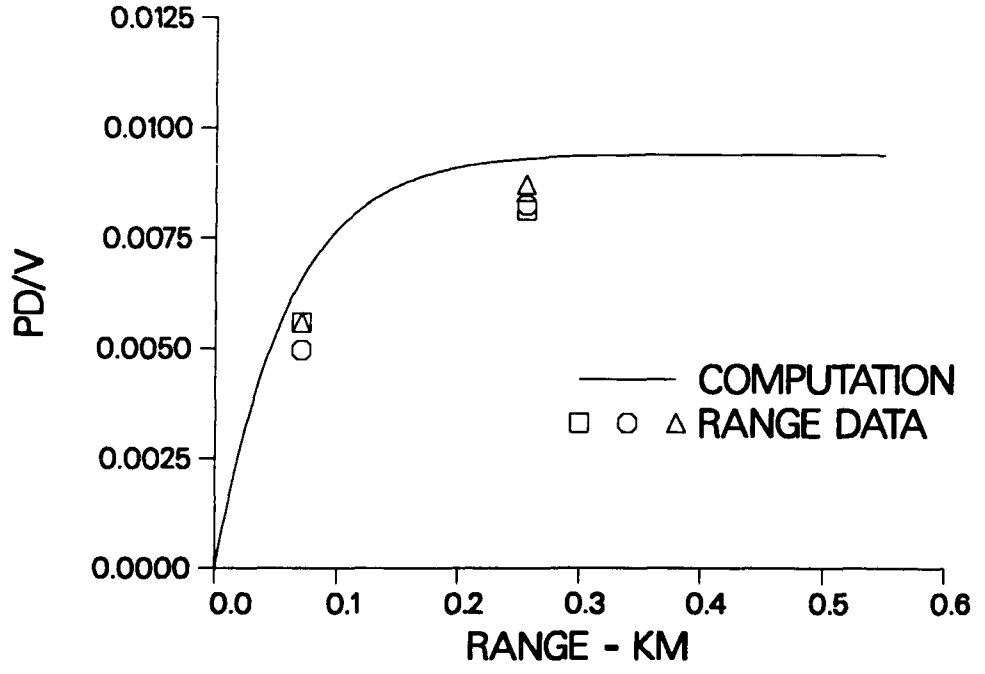

Figure 18. Comparison computed roll history with range data - Launch Mach number = 4.65

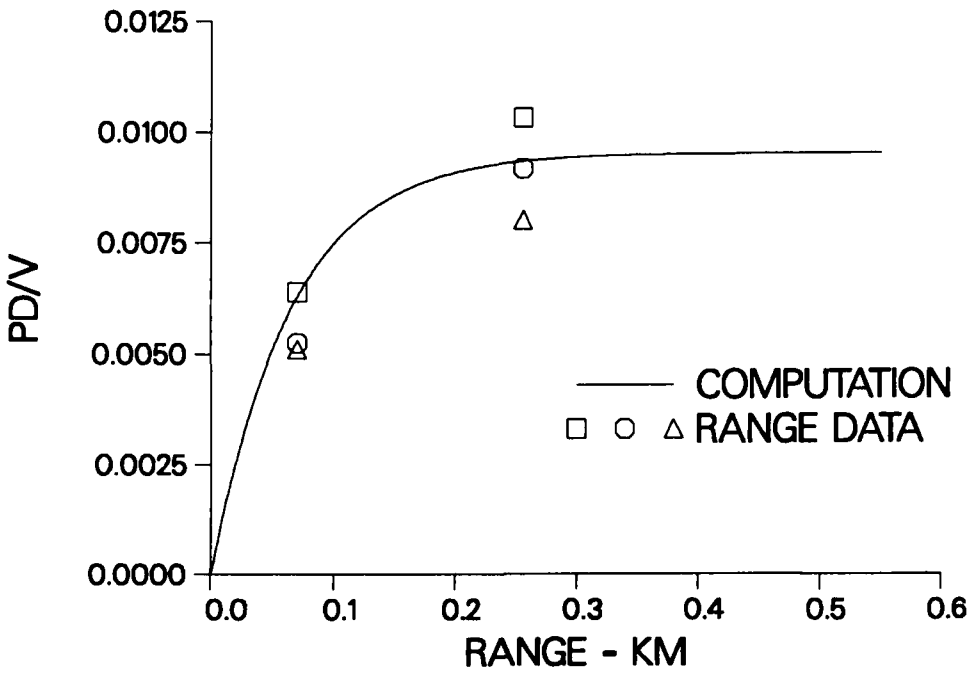

Figure 19. Comparison computed roll history with range data - Launch Mach number = 5.25

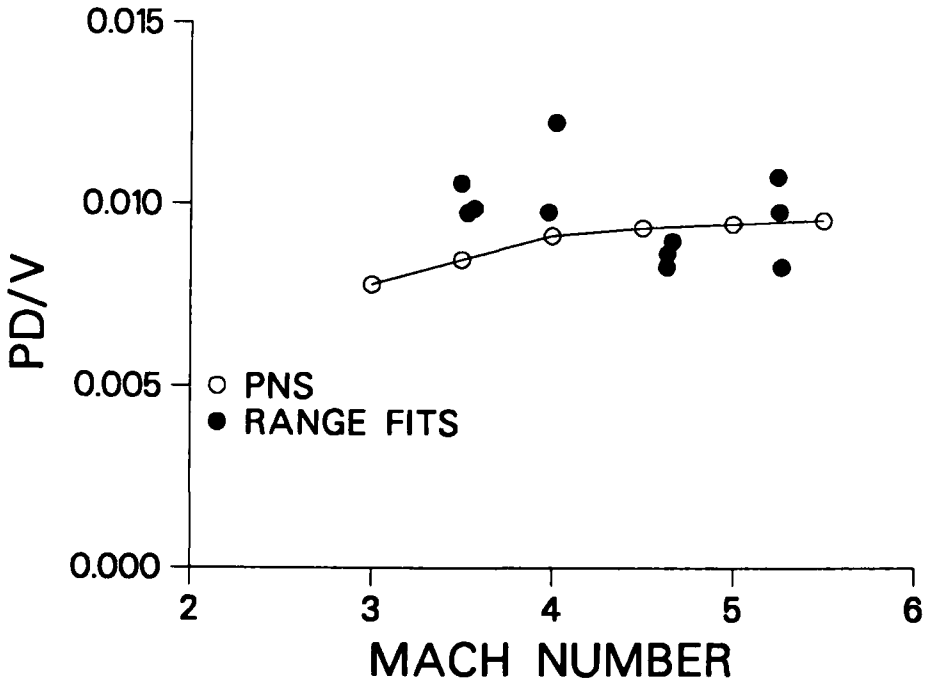

Figure 20. Comparison of computed Mach number variation of equilibrium spin rate with range data

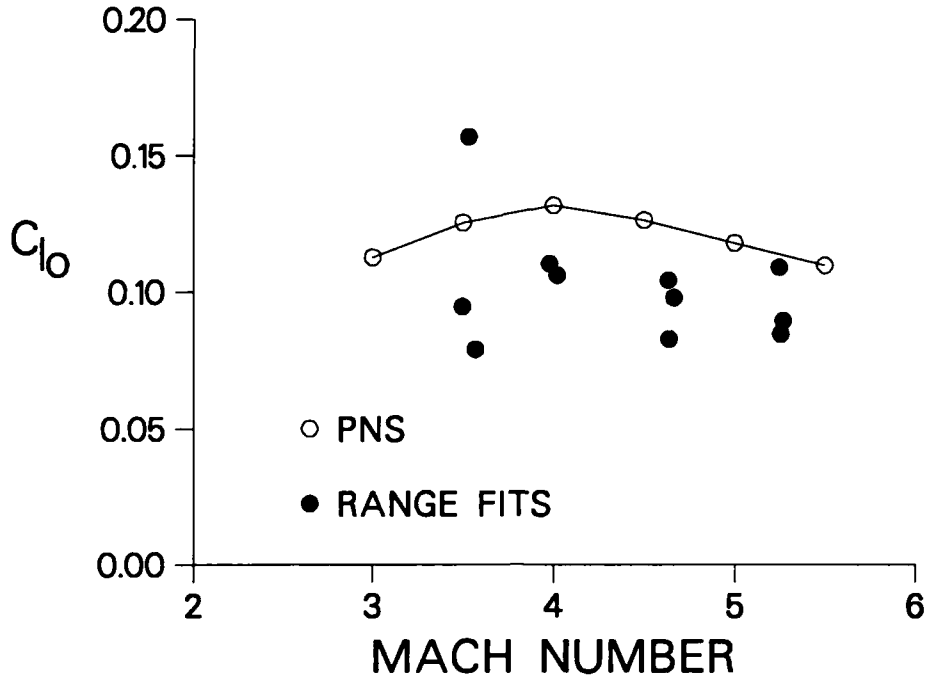

Figure 21. Comparison of computed Mach number variation of roll producing moment coefficient with range data

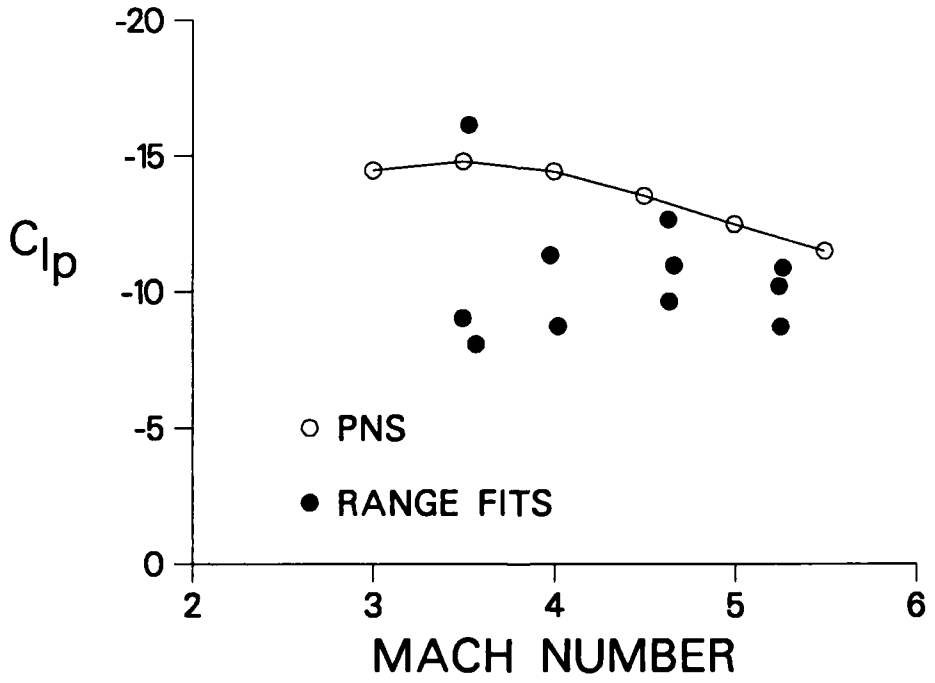

Figure 22. Comparison of computed Mach number variation of roll damping moment coefficient with range data

References

1. Weinacht, P., and Sturek, W.B., "Computation of the Roll Characteristics of Finned Projectiles," U.S. Army Ballistic Research Laboratory, Aberdeen Proving Ground, Maryland, Technical Report BRL-TR-2931, June 1988. (AD 197875)

2. Murphy, C.H., "Free Flight Motion of Symmetric Missiles," U.S. Army Ballistic Research Laboratory, Aberdeen Proving Ground, Maryland, Report No. 1216, July 1963. (AD A442757)

3. Schiff, L.B., and Steger, J.L., "Numerical Simulation of Steady Supersonic Viscous Flow," AIAA Journal, Vol. 18, No. 12, December 1980, pp. 1421-1430.

4. Beam, R., and Warming, R.F., "An Implicit Factored Scheme for the Compressible Navier-Stokes Equations," AIAA Journal, Vol. 16, No. 4, 1978, pp. 85-129.

5. Rai, M.M., and Chaussee, D.S., "New Implicit Boundary Procedure: Theory and Applications," AIAA Paper 83-0123, Reno, Nevada, January 1983.

6. Rai, M.M., and Chaussee, D.S., "Calculation of Viscous Supersonic Flows over Finned Bodies," AIAA Paper 83-1667, Danvers, MA, July 1983.

7. Baldwin, B.S., and Lomax, H., "Thin Layer Approximation and Algebraic Model for Separated Turbulent Flows," AIAA Paper 78-257, 16th Aerospace Sciences Meeting, January, 1978.

8. Brandon, F.J., "Private Communication," U.S. Army Ballistic Research Laboratory, Aberdeen Proving Ground, Maryland

INTENTIONALLY LEFT BLANK.

LIST OF SYMBOLS

a_∞	freestream speed of sound
$c(r)$	local chord length of fin
C_D	drag coefficient
C_l	roll moment coefficient
C_{l_o}	roll producing moment coefficient
C_{l_p}	roll damping moment coefficient
D	projectile diameter
e	total energy per unit volume, normalized by $\rho_\infty a_\infty^2$
$\hat{E}, \hat{F}, \hat{G}$	flux vectors in transformed coordinates
$\hat{H}$	source term resulting from rotating coordinate frame
$\hat{H}_c$	inviscid source term resulting from the cylindrical coordinate formulation
I	moment of inertia
J	Jacobian
L	characteristic length, typically projectile diameter, D
m	projectile mass
M_∞	freestream Mach number
N_{fins}	number of fins
p	pressure, as used in thin-layer Navier-Stokes equations, normalized by $\rho_\infty a_\infty^2$
p	spin rate, as used in the roll equations and aerodynamic coefficients
$\frac{pD}{V}$	nondimensional spin rate
p_∞	freestream static pressure
Re	Reynolds number, $a_\infty \rho_\infty L/\mu_\infty$
r	radial coordinate, normalized by L
s	distance downrange
$\hat{S}$	viscous flux vector in transformed coordinates
$\hat{S}_c$	viscous source term resulting from cylindrical coordinate formulation
S_{ref}	reference cross sectional area of projectile, $\pi D^2/4$
t	time
u,v,w	axial, tangential, and normal velocity components of the Navier-Stokes equations, normalized by a_∞
U,V,W	Contravariant velocities of the transformed Navier-Stokes equations
V	freestream velocity used to non-dimensionalize the spin rate and the aerodynamic coefficients
x	axial coordinate, normalized by L

Greek Symbols

γ	ratio of specific heats
δ(r)	local cant angle of fin
μ	molecular viscosity, normalized by μ_∞
μ_t	turbulent viscosity, normalized by μ_∞
μ_∞	molecular viscosity evaluated at the freestream static temperature
ξ, η, ζ	transformed coordinates
ρ	density, normalized by ρ_∞
ρ_∞	freestream density
Ω	spin rate of rotating coordinate frame, normalized by a_∞/L

INTENTIONALLY LEFT BLANK.

No of Copies	Organization
2	Administrator Defense Technical Info Center ATTN: DTIC-DDA Cameron Station Alexandria, VA 22304-6145
1	HQDA (SARD-TR) WASH DC 20310-0001
1	Commander US Army Materiel Command ATTN: AMCDRA-ST 5001 Eisenhower Avenue Alexandria, VA 22333-0001
1	Commander US Army Laboratory Command ATTN: AMSLC-DL Adelphi, MD 20783-1145
2	Commander US Army, ARDEC ATTN: SMCAR-IMI-I Picatinny Arsenal, NJ 07806-5000
2	Commander US Army, ARDEC ATTN: SMCAR-TDC Picatinny Arsenal, NJ 07806-5000
1	Director Benet Weapons Laboratory US Army, ARDEC ATTN: SMCAR-CCB-TL Watervliet, NY 12189-4050
1	Commander US Army Armament, Munitions and Chemical Command ATTN: SMCAR-ESP-L Rock Island, IL 61299-5000
1	Commander US Army Aviation Systems Command ATTN: AMSAV-DACL 4300 Goodfellow Blvd. St. Louis, MO 63120-1798

No of Copies	Organization
1	Director US Army Aviation Research and Technology Activity ATTN: SAVRT-R (Library) M/S 219-3 Ames Research Center Moffett Field, CA 94035-1000
1	Commander US Army Missile Command ATTN: AMSMI-RD-CS-R (DOC) Redstone Arsenal, AL 35898-5010
1	Commander US Army Tank-Automotive Command ATTN: AMSTA-TSL (Technical Library) Warren, MI 48397-5000
1	Director US Army TRADOC Analysis Command ATTN: ATRC-WSR White Sands Missile Range, NM 88002-5502
(Class. only) 1	Commandant US Army Infantry School ATTN: ATSH-CD (Security Mgr.) Fort Benning, GA 31905-5660
(Unclass. only) 1	Commandant US Army Infantry School ATTN: ATSH-CD-CSO-OR Fort Benning, GA 31905-5660
1	Air Force Armament Laboratory ATTN: AFATL/DLODL Eglin AFB, FL 32542-5000
	Aberdeen Proving Ground
2	Dir, USAMSAA ATTN: AMXSY-D AMXSY-MP, H. Cohen
1	Cdr, USATECOM ATTN: AMSTE-TD
3	Cdr, CRDEC, AMCCOM ATTN: SMCCR-RSP-A SMCCR-MU SMCCR-MSI
1	Dir, VLAMO ATTN: AMSLC-VL-D

No. of Copies	Organization
3	Commander US Army, ARDEC ATTN: SMCAR-CCH-W, A. Warnasch K. Fehsal SMCAR-CCH, J. DeLorenzo Picatinny Arsenal, NJ 07806-5000
1	Commander US Army, ARDEC ATTN: SMCAR-CCH-T, Saif Musalli Picatinny Arsenal, NJ 07806-5000
1	Commander US Army, ARDEC ATTN: SMCAR-CCH-V, Ed Fennell Picatinny Arsenal, NJ 07806-5000
3	Commander US Army, ARDEC ATTN: SMCAR-AET-A, R. Kline J. Grau H. Hudgins Picatinny Arsenal, NJ 07806-5000
3	PEO-Armaments Project Manager Tank Main Armament Systems ATTN: AMCPM-TMA, COL Mullen AMCPM-TMA-105, C. Kimker AMCPM-TMA-120, C. Roller Picatinny Arsenal, NJ 07806-5000
2	Commander Naval Surface Warfare Center Applied Mathematics Branch ATTN: Code R44, Mr. F. Priolo Dr. A. Wardlaw White Oak Laboratory Silver Spring, MD 20903-5000
1	Director Air Force Armament Laboratory AFATL/FXA ATTN: Dr. Dave Belk Eglin AFB, FL 32542-5000
4	Director Air Force Armament Laboratory Aeromechanics Division Aerodynamics Branch ATTN: Mr. Gregg Abate CPT Roger S. Gates Mr. Gerald L. Winchenbach Mr. John R. Cipolla Eglin AFB, FL 32542-5000
1	Director Sandia National Laboratories ATTN: Dr. W. Oberkampf Division 1636 Albuquerque, NM 87185
3	Director NASA Ames Research Center ATTN: M/S N227-8, L. Schiff M/S N258-1, D. Chaussee G. Molvik Moffett Field, CA 94035
2	Honeywell, Inc. ATTN: Mark W. Swenson Richard J. Buretta Mail Station MN48-3700 7225 Northland Drive Brooklyn Park, MN 55428
1	Honeywell, Inc. ATTN: Mark Jones Mail Station MN48-2300 7225 Northland Drive Brooklyn Park, MN 55428
1	Honeywell, Inc. ATTN: Fred Moynihan Defense Systems Division 5901 Lincoln Drive Edina, MN 55436-1678
1	Arrow Technology Associates ATTN: Robert Whyte P.O. Box 4218 Burlington, VT 05491-0042

No. of Copies	Organization
3	General Electric Company Re-Entry Systems Operations ATTN: Dr. James E. Daywitt Dr. David Szostowski Dr. Robert Brewer 3198 Chestnut Street Philadelphia, PA 19101
1	Iowa State University Aerospace Engineering and Engineering Mechanics ATTN: Dr. John O. Ievalts Ames, IA 50011
1	Science and Technology Associates, Inc. ATTN: Mr. Bruce Lohman 4001 North Fairfax Suite 700 Arlington, VA 22203

INTENTIONALLY LEFT BLANK.

USER EVALUATION SHEET/CHANGE OF ADDRESS

This Laboratory undertakes a continuing effort to improve the quality of the reports it publishes. Your comments/answers to the items/questions below will aid us in our efforts.

1. BRL Report Number BRL-TR-3172 Date of Report NOVEMBER 1990

2. Date Report Received _____

3. Does this report satisfy a need? (Comment on purpose, related project, or other area of interest for which the report will be used.) _____

4. Specifically, how is the report being used? (Information source, design data, procedure, source of ideas, etc.) _____

5. Has the information in this report led to any quantitative savings as far as man-hours or dollars saved, operating costs avoided, or efficiencies achieved, etc? If so, please elaborate. _____

6. General Comments. What do you think should be changed to improve future reports? (Indicate changes to organization, technical content, format, etc.) _____

CURRENT ADDRESS

_____
Name

_____
Organization

_____
Address

_____
City, State, Zip Code

7. If indicating a Change of Address or Address Correction, please provide the New or Correct Address in Block 6 above and the Old or Incorrect address below.

OLD ADDRESS

_____
Name

_____
Organization

_____
Address

_____
City, State, Zip Code

(Remove this sheet, fold as indicated, staple or tape closed, and mail.)

----------FOLD HERE----------

DEPARTMENT OF THE ARMY
Director
U.S. Army Ballistic Research Laboratory
ATTN: SLCBR-DD-T
Aberdeen Proving Ground, MD 21005-5066
OFFICIAL BUSINESS

NO POSTAGE
NECESSARY
IF MAILED
IN THE
UNITED STATES

BUSINESS REPLY MAIL
FIRST CLASS PERMIT No 0001, APG, MD

POSTAGE WILL BE PAID BY ADDRESSEE

Director
U.S. Army Ballistic Research Laboratory
ATTN: SLCBR-DD-T
Aberdeen Proving Ground, MD 21005-9989

----------FOLD HERE----------